ACS OMEGA

http://pubs.acs.org/journal/acsodf

Article

Inhibition/Promotion Effect of $C_6F_{12}O$ Addition on Premixed Laminar RP-3/Air Flames

Jin Yu, Fanjun Guo, Binbin Yu,* and Xinsheng Jiang*

Cite This: *ACS Omega* 2023, 8, 3429−3440

Read Online

ACCESS | Metrics & More | Article Recommendations

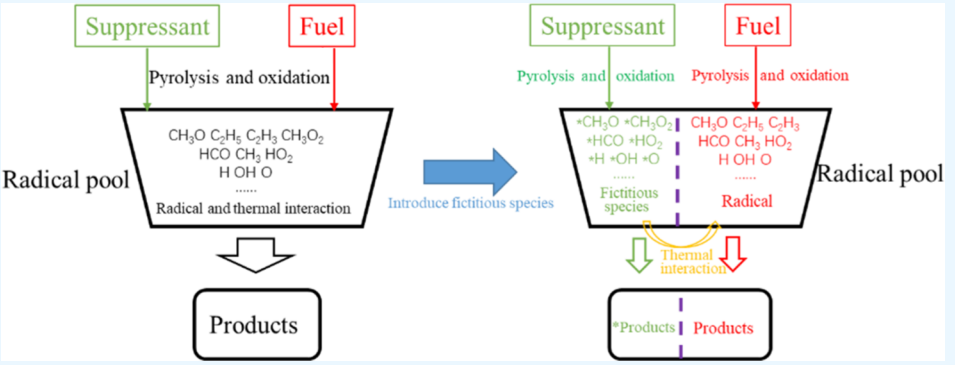

ABSTRACT: $C_6F_{12}O$ (Novec 1230) is one of the most potential substitutes of Halon 1301. However, the study of inhibition/promotion effect of $C_6F_{12}O$ addition on aviation kerosene is rarely reported, which greatly limits the development and application of $C_6F_{12}O$ in oil fire accidents. In this study, numerical research was conducted to study the inhibition/promotion effect of $C_6F_{12}O$ addition by a newly developed and optimized RP-3/$C_6F_{12}O$ coupling skeletal mechanism. A novel methodology based on fictitious species was proposed and adopted to identify the physical dilution and thermal effects as well as the chemical radical and thermal interaction effects of $C_6F_{12}O$ addition. It is observed that both inhibition and promotion effects can be exhibited because the chemical effect includes radical and thermal interactions at different equivalence ratios. In order to explore the kinetic reasons, the reaction path analyses were conducted. The results indicate that the HF formation reactions and the O_2 consumption fluorine-containing reactions, as well as the reactions of $H_2O + F = OH + HF$ and $C_3F_7 + O_2 = C_3F_7O + O$, were the key inhibition and promotion reaction routes, respectively. Compared with methane, the lower H/C ratio of RP-3 makes it more suitable for the use of $C_6F_{12}O$ to suppress combustion.

1. INTRODUCTION

RP-3 jet fuel is a petrochemical aviation kerosene that is widely used in China by military and civilians. However, the RP-3 jet fuel is a typical volatile, flammable, and explosive liquid substance. Once a fire occurs in an oil depot or aircraft, it will cause serious damage. Therefore, the safety of oil in storage, transportation, and use is of great significance to army and the air transport industry. The frequent occurrence of oil and gas explosion accidents has aroused extensive attention of researchers in related fields on the study of oil and gas fire mechanism and its corresponding inhibition technology.

Clean and efficient fire extinguishing is a basic and important research topic in fire research. Halon 1301 (CF_3Br) was used as a high-efficiency extinguishant for various fire accidents. However, the use of Halon 1301 has been discontinued because of its destruction of stratospheric ozone, with exceptions being certain critical applications such as the suppression of cargo-bay fires in aircraft. Therefore, it is imperative to find a new type of fire extinguishing agent as a substitute for Halon. $C_6F_{12}O$ (Novec 1230) is one of the most potential substitutes of Halon 1301, has both physical and chemical fire extinguishing effects, and has gradually gained the attention of the scientists.[1] The physical and chemical effects of $C_6F_{12}O$ addition on methane (CH_4)/air flames have been researched by experimental and numerical methods by Pagliaro et al.[2,3] Similarly, Xu et al.[4] and Ren et al.[5] also investigated the effects of $C_6F_{12}O$ addition on CH_4/air flames by using a counterflow configuration and a numerical method, respectively. Besides, the effect of $C_6F_{12}O$ addition to a lithium-ion cell syngas flame was also investigated by Liu et al.[6] The

Received: November 16, 2022
Accepted: December 23, 2022
Published: January 9, 2023

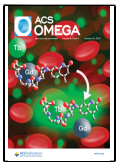

behaviors of unwanted enhancement were observed for the above-mentioned research studies on premixed flames when the fraction of $C_6F_{12}O$ addition is lower than the inerting concentrations. Therefore, investigation of the physical and chemical mechanisms of inhibition/promotion effects is necessary.

In order to comprehensively evaluate the performances of different fire extinguishing agents, analyze the mechanism and conditions of the combustion-promoting phenomenon, and develop the next generation of green composite inhibitors, it is necessary to accurately quantitatively analyze the physicochemical inhibitory effects of fire extinguishing agents. Until now, the quantification of the physicochemical fire extinguishing performance of the inhibitor mainly relies on the numerical simulation based on the chemical reaction mechanism. A methodology to set the suppressant as an inert substance was adopted to quantify the chemical and physical effects by Babushok et al.[7,8] and Ren et al.[5] However, it cannot accurately quantify the pyrolysis effect of the suppressant and the catalytic effect of changing the concentration of radicals by this methodology. Yin et al.[9] separated the detailed promoting and inhibiting effects of combustion from the general chemical effect by replacing a phosphorus-related inhibitor with the corresponding decomposed molecules. However, this method can only approximate the decoupling of the pyrolysis and catalytic effects to a certain extent. Besides, this method is also not universal, and it is difficult to extend to other suppressants. Li et al.[10] proposed a methodology to decouple the thermal and chemical effects of a concerned elementary reaction based on self-modified premix codes. Although this methodology is precise, it is tedious to modify the codes and difficult to extend to other parameter studies. Recently, Liao et al.[11] proposed a methodology that provides a one-step reaction kinetics to fictitious hydrogen addition for separating the hydrogen reactivity effect on radical formation from the heat release effect on flame temperature change. However, for complex fire extinguishing agents, it is very difficult to obtain a high-precision single-step reaction mechanism.

Until now, the inhibition/promotion effect of $C_6F_{12}O$ addition on methane with low carbon molecules has been widely studied. However, for petrochemical aviation kerosene, which consists of hundreds of components including paraffins, aromatics, and so on,[12,13] the study of inhibition/promotion effect of $C_6F_{12}O$ addition on aviation kerosene is rarely reported until now because its composition is too complex. Besides, in order to analyze the inhibition/promotion effect of $C_6F_{12}O$ addition on aviation kerosene, there is an urgent need to propose a simple and accurate methodology to decouple the thermal and radical effects. Moreover, the chemical kinetic mechanism is an indispensable core of combustion simulation, and it is also a key factor to understand how combustion behaves intrinsically.[14] Therefore, it is necessary to investigate the effect of $C_6F_{12}O$ addition on RP-3 flame to fully understand the inhibition/promotion effect on RP-3 combustion intrinsically by the analysis of the chemical kinetic mechanism. Until now, many different reaction mechanisms of RP-3 fuel were proposed and developed.[15−20] However, most of the RP-3 reaction mechanisms are detailed mechanisms, which have very large size and not practical to be used in CFD simulations. Developing a suitable RP-3 skeletal kinetic mechanism coupled with the $C_6F_{12}O$ reaction mechanism for the numerical simulation study is urgently needed.

In summary, the study of the inhibition/promotion effect of $C_6F_{12}O$ addition on aviation kerosene is not reported until now because its composition is too complex. The lack of research studies on the effects of $C_6F_{12}O$ addition on RP-3 greatly limits the development and application of $C_6F_{12}O$ in oil fire accidents. In this study, the skeletal kinetic mechanism of RP-3 coupled with $C_6F_{12}O$ was developed and validated. Then, a novel methodology to decouple the thermal and radical interaction effects based on the fictitious species in the reaction mechanism was proposed to analyze the inhibition/promotion effect of $C_6F_{12}O$ addition on RP-3 fuel. Besides, in order to explore the kinetic reasons, the reaction path analyses were conducted. This study is expected to enrich the fire extinguishing theory and provide theoretical support for the development and application of new fire extinguishing agents.

2. SKELETAL MECHANISM DEVELOPMENT

2.1. Methodology. It is impractical to develop the detailed reaction mechanisms behind each component because RP-3 fuel contains hundreds of hydrocarbon components. The surrogate fuel methodology using several representative components to match the practical fuel's chemical kinetic characteristics is widely used.[21] In our previous works,[22,23] the formulation of RP-3 surrogate fuel which contains 54.3% *n*-dodecane/32.1% 2,5-dimethylhexane/13.6% toluene was proposed by the functional group-based surrogate methodology.[24,25] In this study, this formulation of RP-3 surrogate fuel is adopted. In order to develop a minimal and high-precision RP-3 surrogate mechanism that can be suitable for CFD simulations, a new methodology to develop a kinetic model by integrating a detailed C_0-C_4 core mechanism and a skeletal C_5-C_n mechanism is proposed as inspired by the philosophy of decoupling methodology[26] and updated decoupling methodology.[27] The RP-3 surrogate mechanism was developed by the following strategies: first, to construct sub-mechanisms of *n*-dodecane, 2,5-dimethylhexane and toluene on top of a detailed AramcoMech 3.0 C_0-C_4 core mechanism[28] and then to reduce the size of the detailed C_0-C_4 mechanism by eliminating unimportant species and reactions.

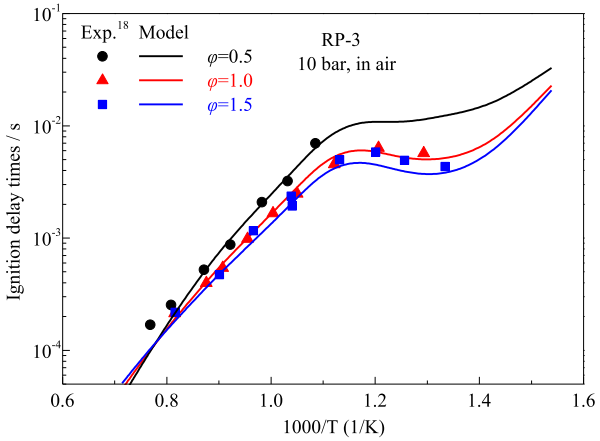

Figure 1. Comparison of the predicted IDTs and the experimental data of RP-3/air. Symbols represent the experimental values of IDTs.[18] Solid lines represent the calculated IDTs of the RP-3 surrogate fuel model.

Subsequently, the kinetic model of $C_6F_{12}O$ developed by Linteris et al.[29] was added into the RP-3 skeletal mechanism.

https://doi.org/10.1021/acsomega.2c07354
ACS Omega 2023, 8, 3429−3440

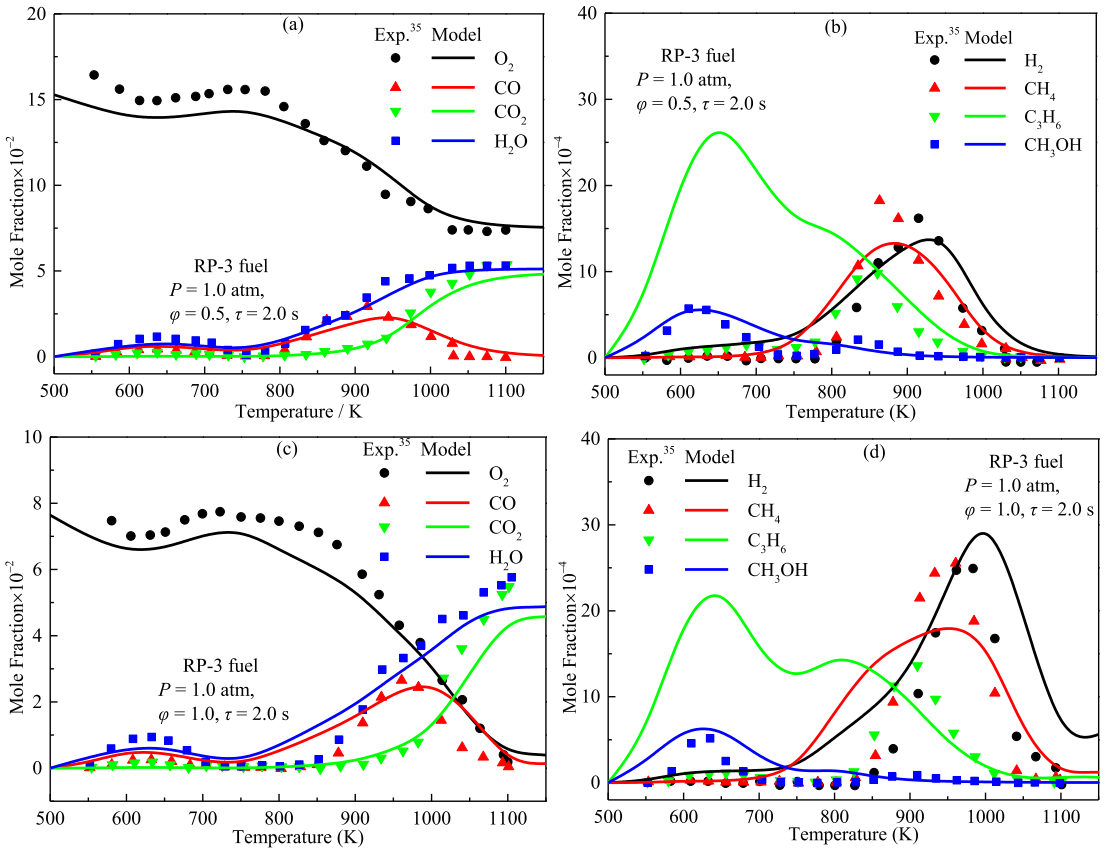

Figure 2. Comparison between the surrogate model predicted values and the experimental data[35] of initial reactants, major intermediate species, and products of RP-3 fuel in JSR. Symbols represent the experimental values.[18] Solid lines represent the computational values of the RP-3 surrogate fuel model.

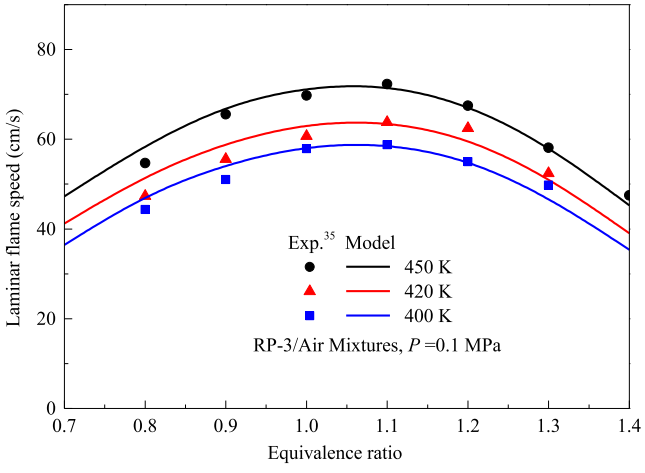

Figure 3. Comparison between the RP-3 model predicted values and the experimental data of the laminar flame speed of RP-3 fuel. Symbols represent the experimental values.[35] Solid lines represent the computational values of the RP-3 surrogate fuel model.

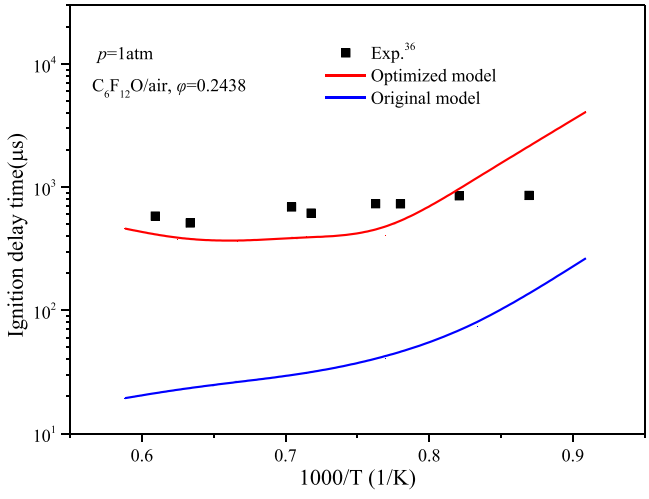

Figure 4. Contrast between $C_6F_{12}O$ IDTs calculated by the original mechanism and the experimental data. Symbols represent the experimental values.[36] Solid lines are computational values.

The reaction mechanism of $C_6F_{12}O$ consists of three parts: (1) the decomposition mechanism of $C_6F_{12}O$ from Linteris et al.,[29] (2) the improved NIST HFC mechanism from Williams et al.,[30] and (3) the C_1-C_4 mechanism proposed by Wang et al.[31] In order to integrate the $C_6F_{12}O$ mechanism and the RP-3 surrogate skeletal mechanism, the decomposition mechanism of $C_6F_{12}O$ and the improved mechanism of NIST HFC were constructed on top of the AramcoMech 3.0 C_0-C_4 core mechanism. Then, the directed relation graphs with error propagation[32] and full species sensitivity analysis[33] kinetic model reduction schemes were used to reduce the size of the detailed C_0-C_4 mechanism. Finally, the reaction mechanism with 191 species and 1242 elementary reactions consisting of four parts, (1) the skeletal C_5-C_n mechanism of *n*-dodecane, 2,5-dimethylhexane, and toluene; (2) the decomposition mechanism of $C_6F_{12}O$; (3) the improved NIST HFC

https://doi.org/10.1021/acsomega.2c07354
ACS Omega 2023, 8, 3429−3440

Table 1. Modification Details of the $C_6F_{12}O$ Mechanism

no.	reactions ($k = AT^n \exp(-E/RT)$)	original A	optimized A
1	$CF_3(+M) = CF_2 + F(+M)$	1.00×10^{15}	1.00×10^{14}
2	$C_2F_5COC_3F_7 => C_3F_7 + C_2F_5CO$	8.50×10^{16}	4.50×10^{15}
3	$C_3F_7 + O = CF_3COF + CF_3$	2.40×10^{13}	3.00×10^{15}
4	$CF_4 + M = CF_3 + F + M$	9.00×10^{34}	2.50×10^{31}
5	$CF_3 + O_2 = CF_3O + O$	2.26×10^{9}	4.26×10^{9}
6	$CF_2 + O_2 = CF_2{:}O + O$	2.00×10^{13}	5.00×10^{11}

mechanism; and (4) the reduced C_0-C_4 core mechanism, has been obtained.

2.2. Validation of the Reaction Mechanism. The multicomponent reaction mechanism should be capable of describing the combustion process of RP-3 fuel and the decomposition/oxidation process of $C_6F_{12}O$ accurately before the validation of describing the mutual effect. Hence, in this section, the RP-3 fuel mechanism and the $C_6F_{12}O$ mechanism were respectively validated against fundamental experiments. The CHEMKIN-II[34] software was used to simulate the combustion process.

2.2.1. Validation of the RP-3 Reaction Mechanism. The ignition delay times (IDTs) of RP-3 fuel were calculated with this surrogate reaction mechanism by using the CHEMKIN-II software. The calculated values were compared to the experimental data of RP-3 fuel, respectively, from Mao et al.[18] and are shown in Figure 1. An increase in equivalence ratio (φ) leading to a decrease in IDT is well reproduced by the RP-3 surrogate model at a low- to high-temperature region. The negative temperature coefficient (NTC) behavior of RP-3 fuel can be clearly observed, and the trend is well reproduced by surrogate model simulation.

The oxidation of RP-3 fuel was investigated by Liu et al.[35] in a jet-stirred reactor (JSR) at pressure (P) = 1.0 atm, φ = 0.5 and 1.0, T = 550−1100 K, and residence time (τ) = 2.0 s. The perfectly stirred reactor model with a transient solver with homogeneous, isothermal, and constant pressure assumptions was used to simulate the species concentration in JSR. Comparisons between the surrogate simulations and experiments of RP-3 fuel for initial reactants, major intermediate species, and products are shown in Figure 2. As shown in Figure 2a−d, at both φ = 0.5 and 1.0, the RP-3 surrogate fuels can accurately predict the evolution of the concentrations of O_2, H_2O, CO, CH_3OH, and CO_2 with the increase of initial temperature. Especially, the NTC behavior from the concentration profiles of initial reactants, major intermediate species, and products is satisfactorily captured by the surrogate fuel from 600 K up to 700 K.

The laminar flame speed of RP-3 fuel was measured by Liu et al.[35] using a constant volume combustion bomb under different unburned gas temperatures and pressures. The PREMIX module in CHEMKIN-II software was used to simulate the laminar flame speed of RP-3 fuel. Comparisons of model predictions and experimental data of the laminar flame speed of RP-3 fuel are shown in Figure 3. The RP-3 skeletal mechanism well reproduces the overall dependence of laminar flame speed on unburned gas temperatures and equivalence ratio. The satisfactory agreement between the predicted and measured laminar flame speed demonstrated the reliability of the reaction mechanism in predicting premixed flames.

2.2.2. Validation of the $C_6F_{12}O$ Reaction Mechanism. Although $C_6F_{12}O$ is a fire extinguishing agent, it still has fuel property which can be oxidized at a fuel-lean condition. The reactions of $C_6F_{12}O$ with oxygen are the key mechanisms to describe and explain the combustion enhancement effect. However, less experimental details about the decomposition/oxidation of $C_6F_{12}O$ are reported in the existing literature studies. Fortunately, the shock tube IDT of $C_6F_{12}O$ at atmospheric pressure and fuel-lean condition was measured by Yu[36] and reported recently. Hence, in this study, the $C_6F_{12}O$ mechanism was validated against this experimental value.

Figure 4 shows the comparison of $C_6F_{12}O$ IDTs calculated by the original mechanism and experimental data[36] at P = 1 atm and φ = 0.24. The original $C_6F_{12}O$ mechanism can capture the evolution trend of IDT on initial temperature but seriously underestimate the IDT at a whole temperature region. In order to improve the prediction accuracy, the $C_6F_{12}O$ mechanism was optimized by adjusting the rate constants of the reactions of $C_6F_{12}O$. In order to find the key reactions that depend on IDT, the sensitivity coefficients of IDT at P = 1 atm and φ = 0.24 were calculated. The top six reactions have been selected to update their rate constants. The optimized reactions and their updated rate constants are shown in Table 1. The performance of the optimized $C_6F_{12}O$ mechanism is also shown in Figure 4. The simulations of the optimized $C_6F_{12}O$ mechanism on the IDT meet the experimental data very well.

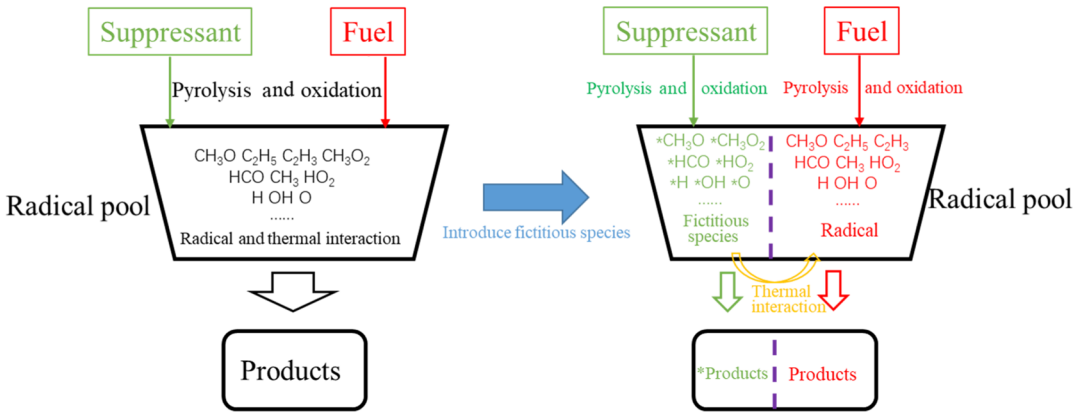

Figure 5. Schematic diagram of the methodology.

https://doi.org/10.1021/acsomega.2c07354
ACS Omega 2023, 8, 3429−3440

3. QUANTITATIVE METHODOLOGY BASED ON FICTITIOUS SPECIES

3.1. Methodology. The reaction process of the inhibitor added in the fuel is shown in Figure 5. When the fuel molecule begins to combust, the macromolecule is first cracked and oxidized, and then many small molecules are further generated. These small molecules contain a large number of free radicals and are called radical pools.[37] Similarly, when the inhibitor is added, it will first be thermally decomposed or oxidized to form many small molecules, which includes a large number of small molecule radicals. In the radical pool, the radicals generated by the inhibitor will interact with the radicals generated by the fuel, and there will also be a large amount of thermal interaction. The radical and thermal interactions will interrupt the propagation of active radicals during the combustion process and inhibit the combustion reaction. In order to decouple the thermal and radical effects of the inhibitor, the concept of fictitious species is introduced, as shown in Figure 5. For this new methodology, all products from the inhibitor mechanism are set as fictitious species and renamed to distinguish them from those generated by the fuel. For example, the H and OH radicals are named *H and *OH in the inhibitor mechanism. In this way, the interaction channel of the radicals between the inhibitor and the fuel is closed, but their own cracking and oxidation paths will not be affected so that the thermal and radical effects of the inhibitor are decoupled.

Table 2. Definition of the Parameters to be Calculated by the Quantization Method

parameter	definition
M_0	combustion parameter value without adding inhibitor
M_1	combustion parameter value of addition of He
M_2	combustion parameter value of addition of the inhibitor at the condition of setting the rate constants of the reactions which involve the inhibitor and their decomposition products to zero
M_3	the combustion parameter value of addition of the inhibitor at the condition of the fictitious species is introduced
M_4	combustion parameter value of addition of the inhibitor
$\Phi(R)$	chemical effect
$\phi(P)$	physical effect
ΔM	change of the combustion parameter
$\phi(P_{Di})$	physical dilution effect
$\phi(P_T)$	physical thermal effect
$\Phi(R_C)$	chemical effect of the radical interaction
$\Phi(R_{De})$	chemical effect of the thermal interaction

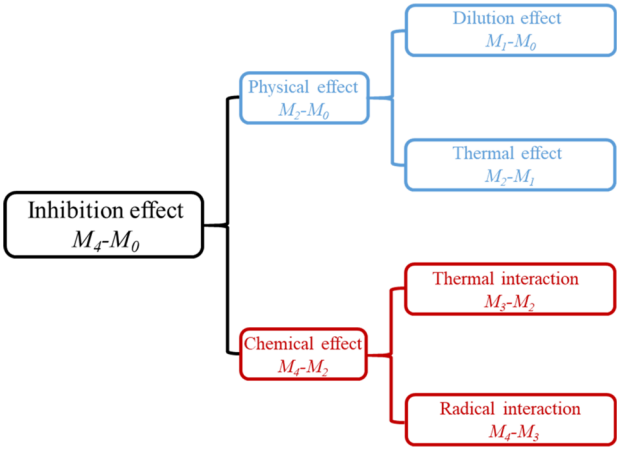

Figure 6. Physical and chemical effects of the inhibitor and their expressions.

3.2. Mathematical Expression. In order to accurately quantify the effects of inhibitors, several parameters were defined and are shown in Table 2. For the convenience of expression, the parameter M is defined to represent the combustion parameters of the fuel, which can be parameters such as the laminar flame speed, IDT, and explosion limit. Five M values, which are represented by $M_0 - M_4$, respectively, need to be calculated under five different conditions. The definitions of $M_0 - M_4$ are shown in Table 2.

Considering the relationship between the physical and chemical effects of inhibitors investigated by Babushok et al.[7,8] and Ren et al.[5] and the additivity principle for estimating the thermodynamic properties of chemicals,[38] this methodology is mathematically expressed as

$$\Delta M = \Phi(R) + \phi(P) \quad (1)$$

where ΔM represents the change of the combustion parameter and $\Phi(R)$ and $\phi(P)$ represent the chemical and physical effects, respectively. Based on eq 1, the definitions of the physical and chemical effects are as follows:

(a) When no inhibitor is added, the combustion parameter value of the fuel is defined as M_0, and the physical and chemical effects of the inhibitor are both 0.

(b) When the inhibitor is added, the combustion parameter value of the fuel is defined as M_4, and the physical and chemical effects of the inhibitor will be shown up simultaneously

$$M_4 - M_0 = \Phi(R) + \phi(P) \quad (2)$$

(c) When the inhibitor is set as an inert substance, the inhibitor only has physical effect, and the physical effect includes dilution and thermal effects

$$M_2 - M_0 = \phi(P) = \phi(P_{Di}) + \phi(P_T) \quad (3)$$

(d) Compared with the inhibitor, the latent heat and specific heat capacity of helium (He) are very low and negligible. It is considered that He only has the dilution effect. When the same amount of He as the inhibitor is added, the inhibitor only plays a diluting role in fuel

$$M_1 - M_0 = \phi(P_{Di}) \quad (4)$$

(e) Then, the physical thermal effect can be solved by eqs 3 and 4

$$M_2 - M_1 = \phi(P_T) \quad (5)$$

(f) Then, the chemical effect which consists of the radical and thermal interactions can be solved by eqs 1 and 2

$$M_4 - M_2 = \phi(R) = \phi(R_C) + \phi(R_{De}) \quad (6)$$

(g) When the fictitious species are introduced through the inhibitor reaction pathway, the effect of the radical interaction is turned off at this time. In addition, the chemical effect of the radical interaction can be defined as

$$M_4 - M_3 = \phi(R_C) \quad (7)$$

https://doi.org/10.1021/acsomega.2c07354
ACS Omega 2023, 8, 3429−3440

(h) Then, the chemical effect of the thermal interaction can be solved by eqs 6 and 7

$$M_3 - M_2 = \phi(R_{De}) \quad (8)$$

The physical and chemical effects of the inhibitor and their expressions are summarized in Figure 6. The physical effect consists of the physical dilution effect and the physical thermal effect. However, the chemical effect consists of the chemical effect of the radical and thermal interactions. All inhibition effects have been quantified exactly by this methodology based on fictitious species.

4. RESULTS AND DISCUSSION

4.1. Physical and Chemical Effects of $C_6F_{12}O$ Addition. In order to analyze the effect of $C_6F_{12}O$ addition on the premixed laminar flame, the laminar flame speeds of RP-3 with different concentrations of $C_6F_{12}O$ addition were calculated and are shown in Figure 7. The volumetric fraction of $C_6F_{12}O$ is calculated by the definition of $V_{C_6F_{12}O}/(V_{C_6F_{12}O} + V_{air})$. Obvious inhibiting effects of $C_6F_{12}O$ addition on RP-3 flame are observed in Figure 7. When the concentration of $C_6F_{12}O$ reaches 4%, the laminar flame speed decreases to less than 3 cm/s at all cases. However, the variation tendency of the laminar flame speed is quite different at different stoichiometric ratios. The laminar flame speed decreases drastically with lower additions of $C_6F_{12}O$ ($\leq$1%), and then, the downtrend slows down at a fuel-rich (φ = 1.4) condition. For φ = 1.0, the laminar flame speed decreases linearly with the increase of $C_6F_{12}O$ when the concentration of $C_6F_{12}O \leq 3\%$, and then the downtrend slows down because of the diminishing marginal benefit between the fire extinguishing performance and concentration when the concentration is more than 3%. For an oxygen-enriched (φ = 0.4) condition, the promotion effect of $C_6F_{12}O$ added on the laminar flame speed of RP-3 is observed. The laminar flame speed increases with the increase of $C_6F_{12}O$ when the concentration of $C_6F_{12}O \leq 1\%$ and then decreases with the increase of $C_6F_{12}O$ when the concentration of $C_6F_{12}O$ >1%. It is concluded that $C_6F_{12}O$ is significantly more effective at fuel-rich and stoichiometric conditions compared to the oxygen-enriched condition.

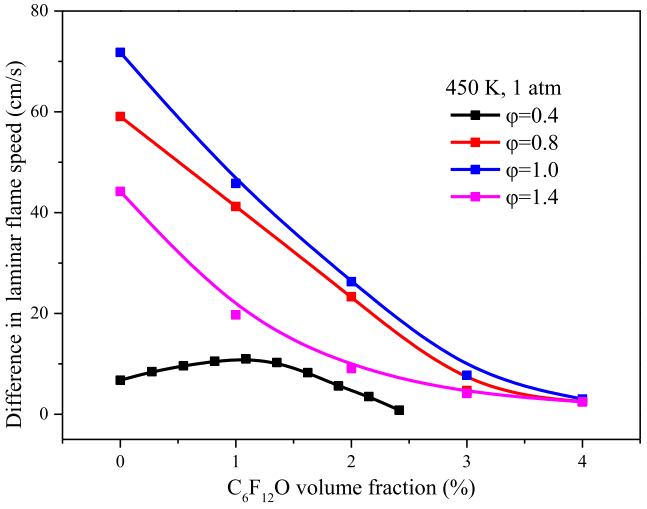

Figure 7. Effect of $C_6F_{12}O$ addition on the laminar flame speed of RP-3 at different φ values.

In order to deeply investigate the mechanism which resulted in the difference performance of $C_6F_{12}O$ at different equivalence ratios, the physical and chemical effects of $C_6F_{12}O$ were identified by the proposed quantitative methodology based on fictitious species. The calculated flame speed change caused by the physical and chemical effects of $C_6F_{12}O$ at different φ values is shown in Figure 8. For the definition of this methodology, a negative value stands for an inhibiting effect on flame speed, whereas a positive value stands for a promoting effect. The total effect stands for the sum of physical and chemical effects. It can be seen that the physical effect of dilution only contributes very little, which is negligible compared to other effects. The physical effect of thermal interaction exhibits an important inhibiting effect under all conditions. In Figure 8a, at a fuel-rich (φ = 1.4) condition, the chemical effect of thermal interaction is a negative value, which means the decomposed reaction of $C_6F_{12}O$ is an endothermic process. With the decrease of φ, the chemical effect of the thermal interaction becomes a positive value (Figure 8b,c). In Figure 8d, at φ = 0.4, the chemical effect of the thermal interaction is the largest influence factor. At φ = 1.4, the chemical effect of the radical interaction is also a negative value. With the decrease of φ, the chemical effect of the radical interaction increases rapidly. However, at φ = 0.4, the chemical effect of the radical interaction promotes flame combustion with lower additions of $C_6F_{12}O$ but inhibits flame combustion when the concentration of $C_6F_{12}O$ > 2%. To sum up, both inhibition and promotion effects can be exhibited as the chemical effect includes radical and thermal interactions at different equivalence ratios.

4.2. Reaction Path Analyses of $C_6F_{12}O$ Addition. The performance of $C_6F_{12}O$ additions on RP-3/air flames is controlled by the competition between its inhibitory properties caused by fluorine reactions and its fuel properties caused by self-oxidation reactions. The effect of $C_6F_{12}O$ addition can be better understood by the variations in the concentration of chain carrier radicals after $C_6F_{12}O$ additions. Therefore, the spatial development of H, OH, and O radicals was investigated and is shown in Figure 9. The values φ = 1.0 and 0.4 are selected for the calculation, which correspond to the case of inhibition and promotion, respectively. For φ = 1.0 (Figure 9a–c), the mole fraction distributions of H, OH, and O radicals decrease with arbitrary addition of $C_6F_{12}O$. However, for φ = 0.4 (Figure 9d–f), the mole fraction distributions of all the radicals increase at a lower addition of $C_6F_{12}O$ (+1%) and then decreased at a higher addition of $C_6F_{12}O$ (+2%).

In order to further explore the kinetics effect on addition of $C_6F_{12}O$, the top 10 elementary reactions affecting the rate of production (ROP) of H, OH, and O radicals were analyzed at φ = 1.0 and with 0 and 3% concentration addition of $C_6F_{12}O$, respectively. Figure 10 shows the main kinetic routes of the production and consumption of these radicals. As shown in Figure 10a,d, with the addition of $C_6F_{12}O$, the reactions of the largest generation and consumption of H radicals $H_2 + OH = H + H_2O$ and $O_2 + H = O + OH$ are replaced by $H_2 + F = H + HF$ and $CF_3 + H = CF_2 + HF$, respectively. HF is an inactive species which can reduce the concentration of the H radical. Therefore, the other two elementary reactions $CF_2 + H = CF + HF$ and $CF_3COF + H = CF_3CO + HF$ play the key roles in H consumption. Similarly, several HF formation reactions, $CF_2 + OH = CF{:}O + HF$, $CF_3 + OH = CF_2{:}O + HF$, and $OH + F = O + HF$, play the key roles in OH consumption (Figure 10b,e). In Figure 10c,f, the O radical is primarily controlled by six

https://doi.org/10.1021/acsomega.2c07354
ACS Omega 2023, 8, 3429−3440

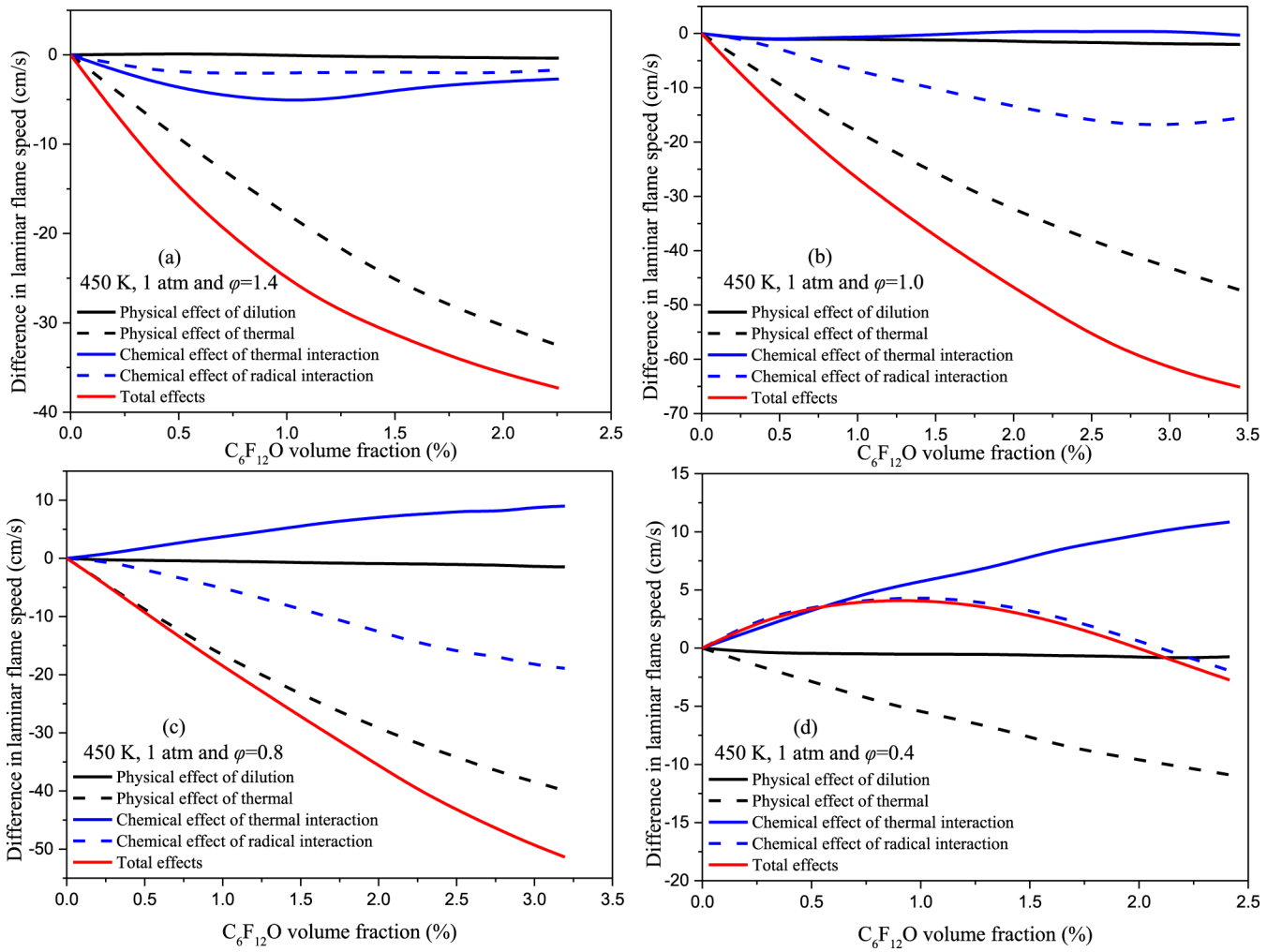

Figure 8. Calculated flame speed change caused by the physical and chemical effects of $C_6F_{12}O$ at φ = (a) 1.4, (b) 1.0, (c) 0.8, and (d) 0.4.

fluorine-containing reactions: CF + O_2 = CF:O + O, C_3F_7 + O_2 = C_3F_7O + O, C_3F_7 + O = CF_3COF + CF_3, CF_2 + O = CF:O + F, CHF + O = CO + HF, and OH + F = O + HF. Two fluorine-containing reactions, CF + O_2 = CF:O + O and C_3F_7 + O_2 = C_3F_7O + O, play the key roles in O production. However, O_2 is scarce at conditions of φ = 1.0. That means, less O_2 can react with H radicals by the chain branching reaction O_2 + H = OH + O, which is the largest generation of O radicals, because of the competition with O_2 by these two fluorine-containing reactions. Therefore, the concentration of the O radical decreases with the addition of $C_6F_{12}O$. To sum up, the HF formation reactions which mostly exhibit the characteristics of chain termination, and the consumption reactions of O_2 which compete O_2 with the chain branching reaction O_2 + H = OH + O, can reduce the concentration of H and OH as well as O radicals, respectively, and thus decrease the laminar flame speed.

The promotion effects of $C_6F_{12}O$ addition on RP-3/air laminar flame speed were found at the oxygen-enriched condition (φ = 0.4). In order to further explore the kinetic mechanism for the promotion behaver of $C_6F_{12}O$ addition under the oxygen-enriched condition, the main kinetic routes of the production and consumption of H, OH, and O radicals were analyzed at φ = 0.4 and with 0 and 1% concentration addition of $C_6F_{12}O$ and are shown in Figure 11. For the 1% $C_6F_{12}O$ addition, only two fluorine-containing reactions, H_2O + F = OH + HF and CF_2 + OH = CF_2:O + H, play the key roles in OH generation and consumption (Figure 11a,d), respectively. The stable oxidative product H_2O becomes an active species by the reaction of H_2O + F = OH + HF, with the addition of $C_6F_{12}O$ (Figure 11b,e). Hence, the concentration of the radical pool will increase with the 1% $C_6F_{12}O$ addition. Besides, a fluorine-containing reaction C_3F_7 + O_2 = C_3F_7O + O plays the key roles in O production (Figure 11c,f). However, different from the condition of φ = 1.0, the reaction of C_3F_7 + O_2 = C_3F_7O + O does not compete O_2 with the other formation reactions of the O radical, O_2 + H = OH + O and C_2H_3 + O_2 = C_2H_2CHO + O, because the O_2 is abundant at φ = 0.4. Therefore, more O radical can be generated with the addition of $C_6F_{12}O$. To sum up, the reaction of H_2O + F = OH + HF which is the main reaction path of the production of the OH radical and C_3F_7 + O_2 = C_3F_7O + O which is the main reaction path of the production of the O radical play the key roles in radical pool generation and thus increase the laminar flame speed.

4.3. Comparison with RP-3 and CH_4 Premixed Laminar Flames. The effects of $C_6F_{12}O$ addition on premixed laminar CH_4/air flames have been widely researched. Hence, the laminar flame speeds of RP-3 fuel and CH_4[3] are compared under the same conditions and are shown in Figure 12. The laminar flame speeds of RP-3 and CH_4 are relatively equal at φ = 1. For φ = 1, both the laminar flame speeds of RP-

https://doi.org/10.1021/acsomega.2c07354
ACS Omega 2023, 8, 3429−3440

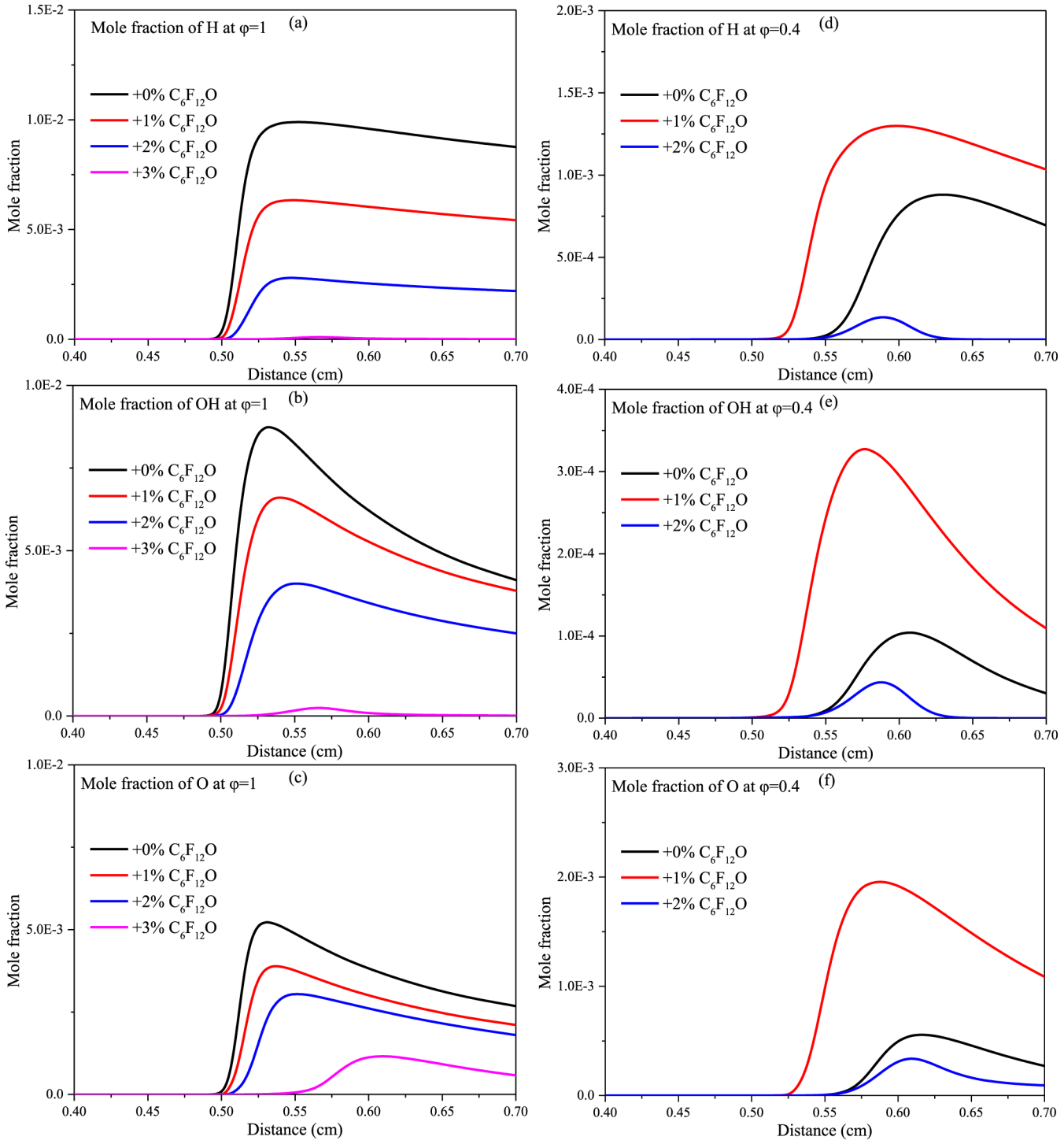

Figure 9. Mole fraction distributions of H, OH, and O radicals with different concentration additions of $C_6F_{12}O$ at φ = (a, b, and c)1.0 and (d, e, and f) 0.4.

3 and CH_4 monotonously decrease with the increase of $C_6F_{12}O$. For φ = 0.6, the laminar flame speeds of RP-3 still monotonously decrease with the increase of $C_6F_{12}O$. However, the promotion effect of $C_6F_{12}O$ addition on CH_4/air flames is observed at low concentration of $C_6F_{12}O$ condition. The laminar flame speed increases with the increase of $C_6F_{12}O$ when the concentration of $C_6F_{12}O \leq 2\%$ and then decreases with the increase of $C_6F_{12}O$ when the concentration of $C_6F_{12}O > 2\%$. It can be seen from the previous introduction that the promotion effect of $C_6F_{12}O$ addition on the laminar flame speed of RP-3 occurs at φ = 0.4, which is lower than that of CH_4.

The above studies indicate that the promotion effect of $C_6F_{12}O$ addition on the CH_4 flame is formed more easily than RP-3. From the above analysis on the kinetic effect of $C_6F_{12}O$ addition, we can see that the reaction of $H_2O + F = OH + HF$ is the main reaction path of the production of the OH radical, which plays the key role in radical pool generation and thus increases the laminar flame speed. In order to illustrate the reason why CH_4 is easy to promote the combustion process at

https://doi.org/10.1021/acsomega.2c07354
ACS Omega 2023, 8, 3429−3440

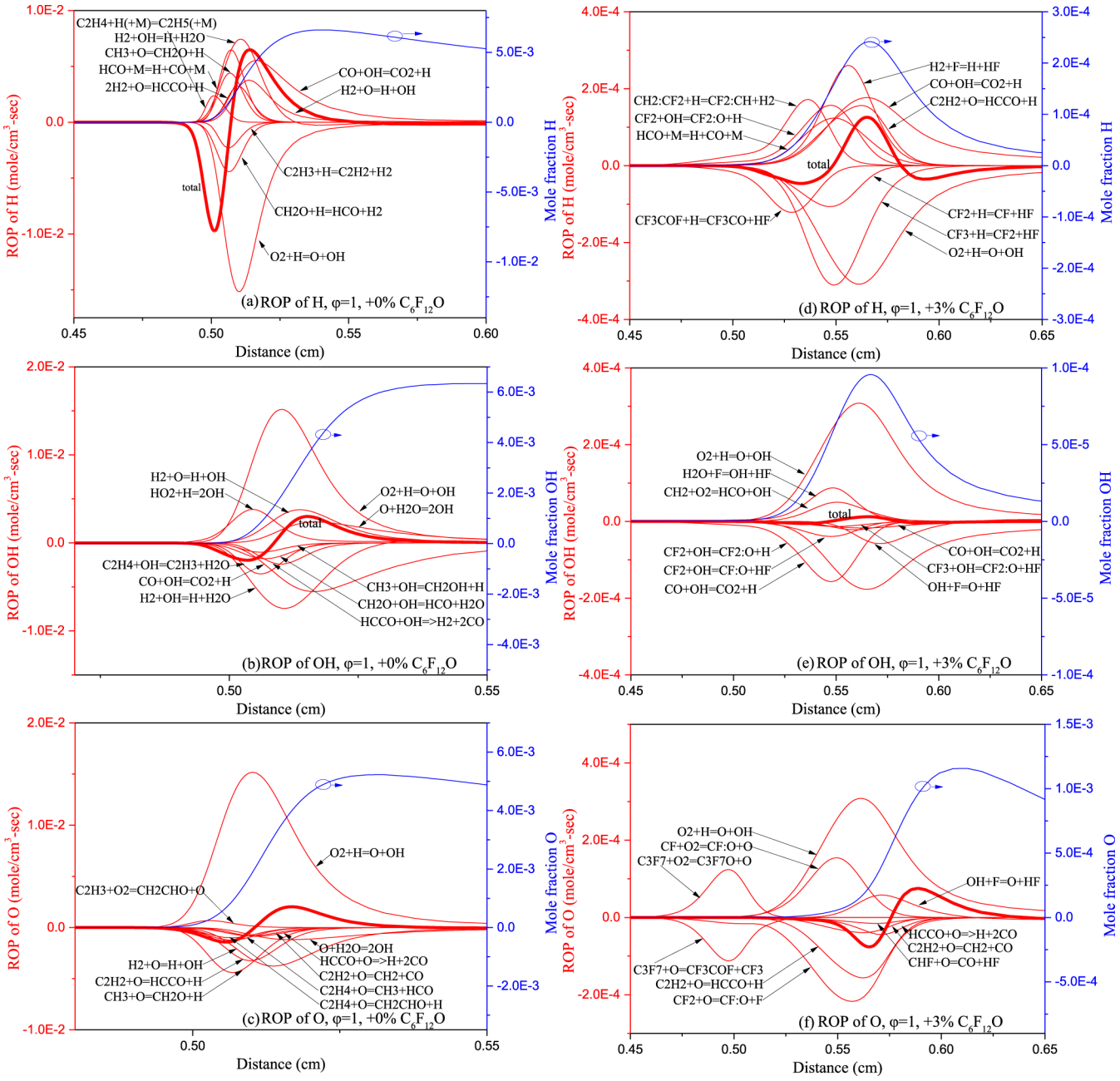

Figure 10. Contributions of main elementary reactions to ROP of (a and d) H, (b and e) OH, and (c and f) O radicals with different concentration additions of $C_6F_{12}O$ at φ = 1.0.

an oxygen-enriched environment, the mole fraction distributions of H_2O and OH radical for RP-3 and CH_4 with different concentration additions of $C_6F_{12}O$ were calculated and are shown in Figure 13. The $CH_4/C_6F_{12}O$-coupled mechanism of Linteris et al.[29] was adopted to calculate the species distribution. From Figure 13a, it can be seen that the mole fraction of H_2O for CH_4 is much higher than that of RP-3 when no $C_6F_{12}O$ is added. The concentration of H_2O in flame is controlled by the hydrogen/carbon (H/C) ratio of fuel. The H/C ratios of RP-3 and CH_4 are, respectively, 2.09 and 4.0, which means more H_2O can be generated for CH_4. As discussed in ref 39, the rate of the reaction $H_2O + F = OH + HF$ increases as the concentration of H_2O increases. Not only is this reaction exothermic, it also forms the active flame radial OH. Therefore, the rate of the reaction $H_2O + F = OH + HF$ for CH_4 is much greater than RP-3 because of the higher concentration of H_2O for CH_4. Hence, the increase of the mole fraction of OH for CH_4 is observed in Figure 13b. However, the increase of the generated OH by the reaction $H_2O + F = OH + HF$ for RP-3 is very limited, and the formation reactions of HF which mostly exhibit the characteristics of chain termination play the leading roles in radical pool generation and thus decrease the laminar flame speed. Therefore, the lower H/C ratio of RP-3 makes it more suitable than CH_4 for the use of $C_6F_{12}O$ to suppress combustion.

5. CONCLUSIONS

The skeletal kinetic mechanism of RP-3 coupled with $C_6F_{12}O$ reaction chemistry was developed and validated. Based on the

https://doi.org/10.1021/acsomega.2c07354
ACS Omega 2023, 8, 3429−3440

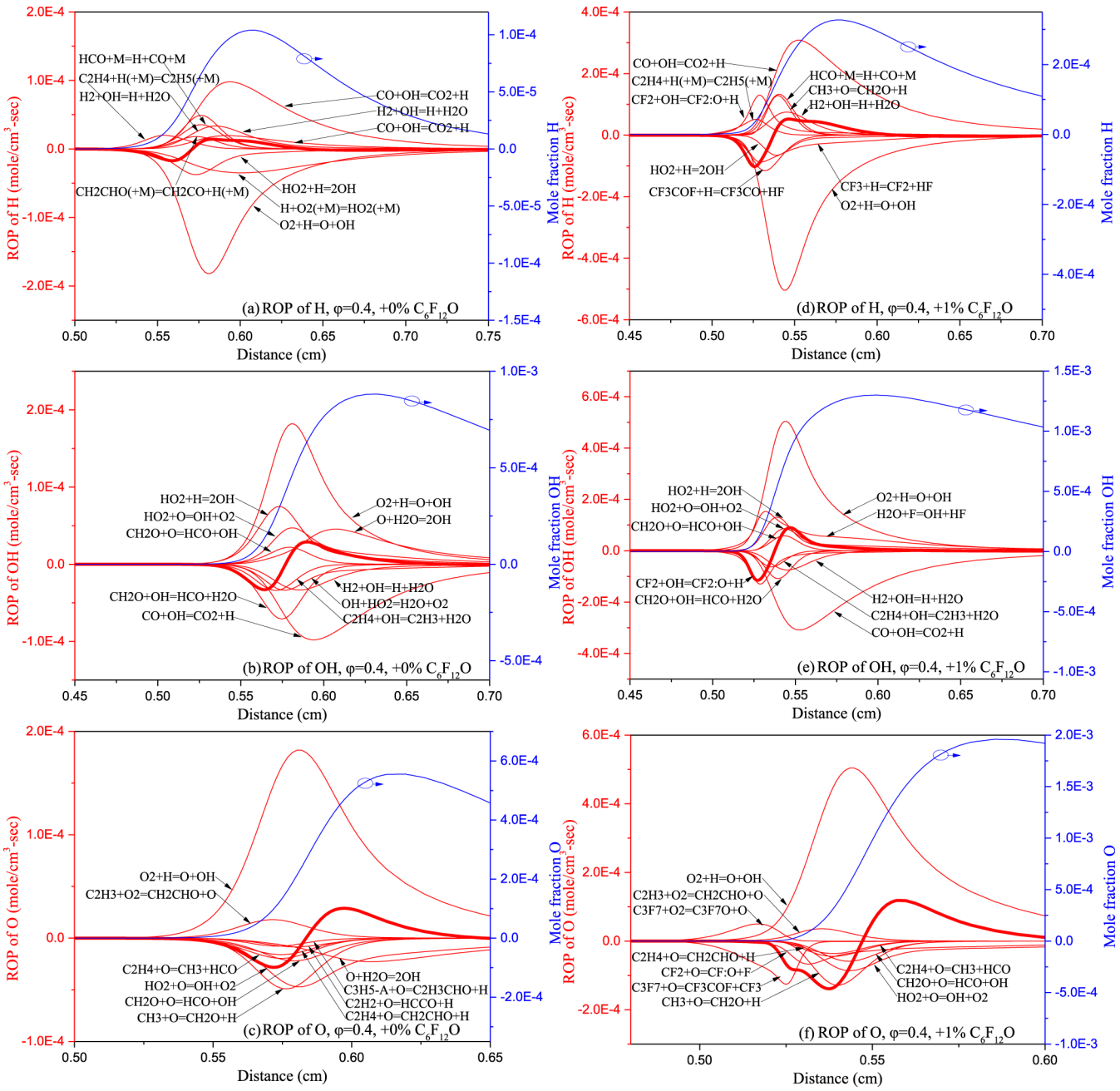

Figure 11. Contributions of main elementary reactions to ROP of (a and d) H, (b and e) OH, and (c and d) O radicals with different concentration additions of $C_6F_{12}O$ at φ = 0.4.

latest experiment, the $C_6F_{12}O$ mechanism was optimized by adjusting the rate constants. Then, a novel methodology to decouple the thermal and radical interaction effects based on fictitious species in the kinetic mechanism was proposed to analyze the inhibition/promotion effect of $C_6F_{12}O$ addition on RP-3 flame. The main conclusions are given as follows:

(1) The thermal and radical interaction effects of $C_6F_{12}O$ addition on RP-3 flame were accurately quantized by this novel methodology based on fictitious species. The results show that the thermal interaction exhibits an inhibiting effect at the fuel-rich condition. With the increase of oxygen, the thermal interaction gradually exhibits the effect of promoting combustion. The radical interaction effect on inhibiting the flame is gradually enhanced with the decrease of φ. However, the radical interaction effect plays promoting roles in the oxygen-enriched condition.

(2) The reaction path of $C_6F_{12}O$ addition was investigated. The formation reactions of HF and the O_2 consumption fluorine-containing reactions can decrease the concentration of radicals and thus decrease the laminar flame speed. However, the enhanced production of OH by $H_2O + F = OH + HF$ and the enhanced production of O by $C_3F_7 + O_2 = C_3F_7O + O$ are the reaction paths of $C_6F_{12}O$ addition to promote the oxidation of RP-3 flame at the oxygen-enriched condition.

(3) The H/C ratio of CH_4 is higher than that of RP-3, which means a higher concentration of H_2O can be generated, and thus increases the rate of $H_2O + F = OH + HF$. Therefore, the promotion combustion effect of $C_6F_{12}O$

https://doi.org/10.1021/acsomega.2c07354
ACS Omega 2023, 8, 3429−3440

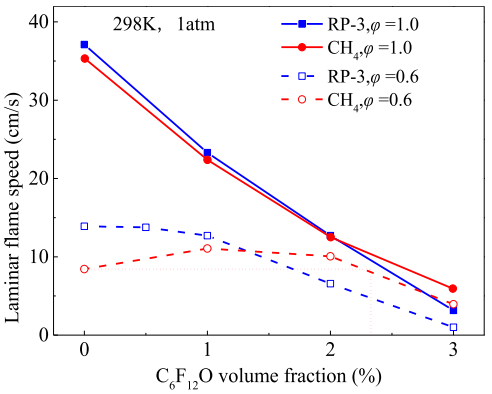

Figure 12. Effect of $C_6F_{12}O$ addition on the laminar flame speed of RP-3 and CH_4.

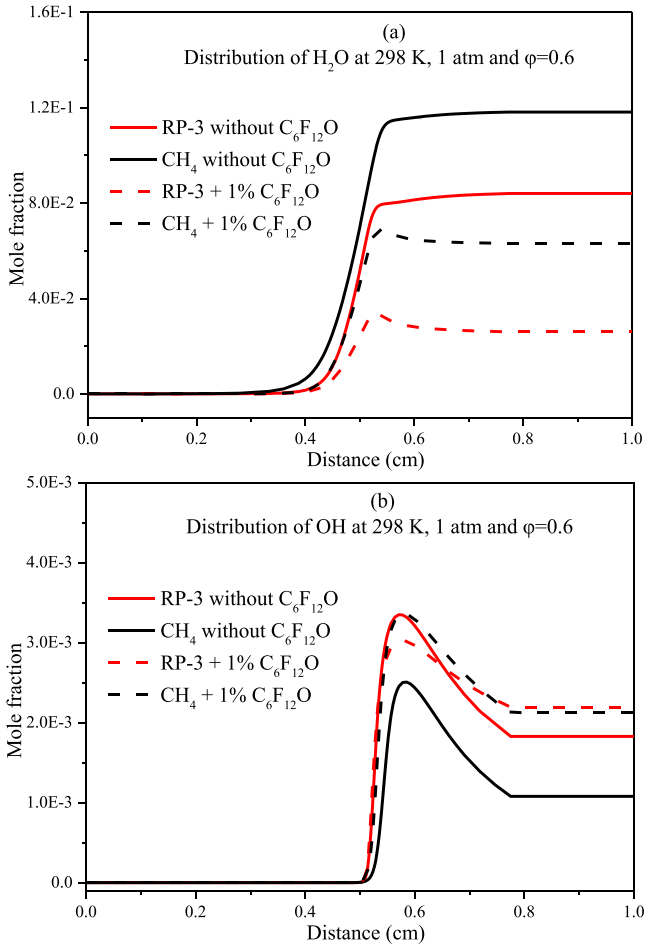

Figure 13. Mole fraction distributions of (a) H_2O and (b) OH radical for RP-3 and CH_4.

added on the CH_4 laminar flame is more intense than that if RP-3 at the same oxygen-enriched condition.

AUTHOR INFORMATION

Corresponding Authors

Binbin Yu − *Petroleum, Oil&Lubricants Department in Army Logistics Academy of PLA, Chongqing 401331, China;* orcid.org/0000-0003-1702-6189; Email: yubb19@sina.com

Xinsheng Jiang − *Petroleum, Oil&Lubricants Department in Army Logistics Academy of PLA, Chongqing 401331, China;* Email: jxs_dy@163.com

Authors

Jin Yu − *Petroleum, Oil&Lubricants Department in Army Logistics Academy of PLA, Chongqing 401331, China; School of Aeronautics, Chongqing Jiaotong University, Chongqing 400074, China; Chongqing Key Laboratory of Green Aviation Energy and Power, Chongqing 401120, China; The Green Aerotechnics Research Institute of Chongqing Jiaotong University, Chongqing 401120, China;* orcid.org/0000-0001-5695-6886

Fanjun Guo − *School of Aeronautics, Chongqing Jiaotong University, Chongqing 400074, China*

Complete contact information is available at: https://pubs.acs.org/10.1021/acsomega.2c07354

Notes

The authors declare no competing financial interest.

ACKNOWLEDGMENTS

This work was supported by the National Natural Science Foundation of China (no. 52006020), the Chongqing Research Program of Basic Research and Frontier Technology (no. cstc2019jcyj-msxm1610), and the Open Fund of Chongqing Key Laboratory of Fire and Explosion Safety (The Evaluating Laboratory of Military Oil Depot Safety and Facility Equipment) (no. LQ21KFJJ04).

REFERENCES

(1) Xing, H.; Lu, S.; Yang, H.; Zhang, H. Review on research progress of C6F12O as a fire extinguishing agent. *Fire* **2022**, *5*, 50.

(2) Pagliaro, J. L.; Linteris, G. T.; Sunderland, P. B.; Baker, P. T. Combustion inhibition and enhancement of premixed methane−air flames by halon replacements. *Combust. Flame* **2015**, *162*, 41−49.

(3) Pagliaro, J.; Linteris, G. Hydrocarbon flame inhibition by C6F12O (Novec 1230): Unstretched burning velocity measurements and predictions. *Fire Saf. J.* **2017**, *87*, 10−17.

(4) Xu, W.; Jiang, Y.; Ren, X. Combustion promotion and extinction of premixed counterflow methane/air flames by C6F12O fire suppressant. *J. Fire Sci.* **2016**, *34*, 289−304.

(5) Ren, X.; Jiang, Y.; Xu, W. Numerical investigation of the chemical and physical effects of halogenated fire suppressants addition on methane-air mixtures. *J. Fire Sci.* **2016**, *34*, 416−430.

(6) Liu, L.; Du, Z.; Zhang, T.; Guo, Z.; He, M.; Liu, Z. The inhibition/promotion effect of C6F12O added to a lithium-ion cell syngas premixed flame. *Int. J. Hydrogen Energy* **2019**, *44*, 22282−22300.

(7) Babushok, V.; Tsang, W.Chemical and physical influences of halogenated fire suppressants. *Proceedings of the 7th HOTWC, NIST special pub. 984-2*, 1997; Vol. *55*.

(8) Noto, T.; Babushok, V.; Hamins, A.; Tsang, W. Inhibition effectiveness of halogenated compounds. *Combust. Flame* **1998**, *112*, 147−160.

(9) Yin, Y.; Jiang, Y.; Qiu, R.; Xiong, C. Physical and chemical effects of phosphorus-containing compounds on laminar premixed flame. *Chin. Phys. B* **2018**, *27*, 094701.

(10) Li, W.; Jiang, Y.; Xia, Y.Numerical Study on Decoupling the Chemical and Thermal Effects of a Specific Elementary Reaction on the Laminar Flame Speed. *Proceedings of the Ninth International Seminar on Fire and Explosion Hazards*, 2019.

(11) He, Y.; Liang, M.; Liao, S.; Jian, X.; Shao, Y.; Jin, Z. Chemical effects of hydrogen addition on low-temperature oxidation of premixed laminar methane/air flames. *Fuel* **2020**, *280*, 118600.

https://doi.org/10.1021/acsomega.2c07354
ACS Omega 2023, 8, 3429−3440

(12) Huber, M.; Smith, B.; Ott, L.; Bruno, T. Surrogate mixture model for the thermophysical properties of synthetic aviation fuel S-8: Explicit application of the advanced distillation curve. *Energy Fuels* **2008**, *22*, 1104−1114.
(13) Widegren, J. A.; Bruno, T. J. Thermal decomposition kinetics of the aviation turbine fuel Jet A. *Ind. Eng. Chem. Res.* **2008**, *47*, 4342−4348.
(14) Dryer, F. L. Chemical kinetic and combustion characteristics of transportation fuels. *Proc. Combust. Inst.* **2015**, *35*, 117−144.
(15) Zheng, D.; Yu, W.-M.; Zhong, B.-J. RP-3 aviation kerosene surrogate fuel and the chemical reaction kinetic model. *Acta Phys.-Chim. Sin.* **2015**, *31*, 636−642.
(16) Xu, J.-Q.; Guo, J. J.; Liu, A. K.; Wang, J. L.; Tan, N. X.; Li, X. Y. Construction of Autoignition Mechanisms for the Combustion of RP-3 Surrogate Fuel and Kinetics Simulation. *Acta Phys.-Chim. Sin.* **2015**, *31*, 643.
(17) Yi, R.; Chen, X.; Chen, C. Surrogate for emulating physicochemical and kinetics characteristics of RP-3 aviation fuel. *Energy Fuels* **2019**, *33*, 2872−2879.
(18) Mao, Y.; Yu, L.; Wu, Z.; Tao, W.; Wang, S.; Ruan, C.; Zhu, L.; Lu, X. Experimental and kinetic modeling study of ignition characteristics of RP-3 kerosene over low-to-high temperature ranges in a heated rapid compression machine and a heated shock tube. *Combust. Flame* **2019**, *203*, 157−169.
(19) Li, A.; Zhang, Z.; Cheng, X.; Lu, X.; Zhu, L.; Huang, Z. Development and validation of surrogates for RP-3 jet fuel based on chemical deconstruction methodology. *Fuel* **2020**, *267*, 116975.
(20) Zeng, W.; Li, H.-x.; Chen, B.-d.; Ma, H.-a. Experimental and kinetic modeling study of ignition characteristics of Chinese RP-3 kerosene. *Combust. Sci. Technol.* **2015**, *187*, 396−409.
(21) Pitz, W. J.; Mueller, C. J. Recent progress in the development of diesel surrogate fuels. *Prog. Energy Combust. Sci.* **2011**, *37*, 330−350.
(22) Yu, J.; Gou, X. Comprehensive Surrogate for Emulating Physical and Kinetic Properties of Jet Fuels. *J. Propul. Power* **2017**, *34*, 679−689.
(23) Yu, J.; Tang, G.-Z.; Yu, J.-J. Detailed combustion chemical mechanism for surrogates of representative jet fuels. *J. Energy Inst.* **2020**, *93*, 2421−2434.
(24) Yu, J.; Ju, Y.; Gou, X. Surrogate fuel formulation for oxygenated and hydrocarbon fuels by using the molecular structures and functional groups. *Fuel* **2016**, *166*, 211−218.
(25) Yu, J.; Cao, J.-m.; Yu, J.-j. The development of F-76 and algae-derived HRD-76 diesel fuel surrogates. *Fuel* **2021**, *302*, 121075.
(26) Chang, Y.; Jia, M.; Li, Y.; Liu, Y.; Xie, M.; Wang, H.; Reitz, R. D. Development of a skeletal mechanism for diesel surrogate fuel by using a decoupling methodology. *Combust. Flame* **2015**, *162*, 3785−3802.
(27) Zhang, X.; Mani Sarathy, S. M. A lumped kinetic model for high-temperature pyrolysis and combustion of 50 surrogate fuel components and their mixtures. *Fuel* **2021**, *286*, 119361.
(28) Zhou, C.-W.; Li, Y.; Burke, U.; Banyon, C.; Somers, K. P.; Ding, S.; Khan, S.; Hargis, J. W.; Sikes, T.; Mathieu, O. An experimental and chemical kinetic modeling study of 1, 3-butadiene combustion: Ignition delay time and laminar flame speed measurements. *Combust. Flame* **2018**, *197*, 423−438.
(29) Linteris, G. T.; Babushok, V. I.; Sunderland, P. B.; Takahashi, F.; Katta, V. R.; Meier, O. Unwanted combustion enhancement by C6F12O fire suppressant. *Proc. Combust. Inst.* **2013**, *34*, 2683−2690.
(30) Williams, B. A.; Espérance, D.; Fleming, J. W. Intermediate species profiles in low-pressure methane/oxygen flames inhibited by 2-H heptafluoropropane: comparison of experimental data with kinetic modeling. *Combust. Flame* **2000**, *120*, 160−172.
(31) Wang, H.; You, X.; Joshi, A. V.; Davis, S. G.; Laskin, A.; Egolfopoulos, F.; Law, C.*USC Mech Version II. High-Temperature Combustion Reaction Model of H2/CO/C1-C4 Compounds*, 2007, http://ignis.usc.edu/USC_Mech_II.htm.
(32) Chen, Y.; Chen, J.-Y. Application of Jacobian defined direct interaction coefficient in DRGEP-based chemical mechanism reduction methods using different graph search algorithms. *Combust. Flame* **2016**, *174*, 77−84.
(33) Stagni, A.; Frassoldati, A.; Cuoci, A.; Faravelli, T.; Ranzi, E. Skeletal mechanism reduction through species-targeted sensitivity analysis. *Combust. Flame* **2016**, *163*, 382−393.
(34) Kee, R. J.; Rupley, F. M.; Miller, J. A.*Chemkin-II: A Fortran Chemical Kinetics Package for the Analysis of Gas-Phase Chemical Kinetics*; Sandia National Lab.(SNL-CA): Livermore, CA (United States), 1989.
(35) Liu, J.; Hu, E.; Yin, G.; Huang, Z.; Zeng, W. An experimental and kinetic modeling study on the low-temperature oxidation, ignition delay time, and laminar flame speed of a surrogate fuel for RP-3 kerosene. *Combust. Flame* **2022**, *237*, 111821.
(36) Yu, B.*Study on Combustion and Suppression Mechanism of No. 3 Jet Fuel Based on Chemical Dynamics*. Army Logistics Acadamy of PLA, 2022.
(37) Dooley, S.; Won, S. H.; Heyne, J.; Farouk, T. I.; Ju, Y.; Dryer, F. L.; Kumar, K.; Hui, X.; Sung, C.-J.; Wang, H.; Oehlschlaeger, M. A.; Iyer, V.; Iyer, S.; Litzinger, T. A.; Santoro, R. J.; Malewicki, T.; Brezinsky, K. The experimental evaluation of a methodology for surrogate fuel formulation to emulate gas phase combustion kinetic phenomena. *Combust. Flame* **2012**, *159*, 1444−1466.
(38) Reid, R. C.; Prausnitz, J. M.; Poling, B. E.*The Properties of Gases and Liquids*; U.S. Department of Energy Office of Scientific and Technical Information, 1987.
(39) Babushok, V. I.; Linteris, G. T.; Baker, P. T. Influence of water vapor on hydrocarbon combustion in the presence of hydrofluorocarbon agents. *Combust. Flame* **2015**, *162*, 2307−2310.

https://doi.org/10.1021/acsomega.2c07354
ACS Omega 2023, 8, 3429−3440